Heritage Science

RESEARCH ARTICLE

Open Access

The synergistic effect of an imidazolium salt and benzotriazole on the protection of bronze surfaces with chitosan-based coatings

Debora Kelen Silva da Conceição[1], Kauana Nunes de Almeida[1], Elsa Nhuch[1], Maria Grazia Raucci[2], Chiara Santillo[3], Martina Salzano de Luna[3,4], Luigi Ambrosio[2], Marino Lavorgna[3], Chiara Giuliani[5], Gabriella Di Carlo[5], Maria Paola Staccioli[5], Tiago Falcade[6] and Henri Stephan Schrekker[1*]

Abstract

The class of imidazolium salts contains effective anticorrosion additives for metal substrates. This study evaluated the potential of 1-carboxymethyl-3-methylimidazolium bis (trifluoromethylsulfonyl) imide (**$HO_2CC_1MImNTf_2$**) for application in cultural heritage, exploring it as anticorrosion additive in chitosan-based coatings for the protection of copper-based alloys. Under accelerated corrosion conditions with HCl vapor, the chitosan coating with **$HO_2CC_1MImNTf_2$** was less effective than the one with benzotriazole. The coating with a combination of **$HO_2CC_1MImNTf_2$** and benzotriazole resulted in the optimal protective efficacy of the bronze surface, and it also maintained high transparency without changing the bronze appearance.

Keywords: Biopolymer matrix, Anticorrosive, Copper-based alloy artifact, Ionic liquid

Introduction

Corrosion phenomena affecting metal surfaces exposed in polluted environments represent a serious global problem in several areas [1]. In the field of Cultural Heritage, for example, copper-based alloys have been widely used as raw materials by important artists in the last decades. Copper-based artworks, like other common metal objects, are subjected to corrosion processes due to the reaction of the metal surface with aggressive species present in the surrounding environment. The deterioration phenomena lead to the formation of both stable protective and reactive degrading species. Their chemical composition is mainly influenced by the composition of the alloy itself and by the environmental agents that come in contact with the object [1–5]. The corrosion products affect the aesthetical appearance of artworks and can compromise their structural properties [6].

Not only atmospheric pollutants, moisture or marine aerosol from outdoor environment can start the degradation processes. Aggressive species such as volatile organic compounds, particularly acetic and formic acid, or hydrogen sulphide, can be also present in indoor environments due to inadequate aeration, human emission, dust, construction materials and furniture.

For these reasons, metals substrates have to be protected to avoid degradation reactions and the formation of undesired products. Oxygen, humidity and chloride ions are particularly aggressive towards copper-based substrates since they induce a cyclic and irreversible degradation process known as "bronze disease". It leads to the formation of corrosion products based on atacamite and its polymorphs ($Cu_2(OH)_3Cl$), which are mainly responsible for the transformation of the alloy in a greenish powder. Moisture and oxygen cause also the formation of cuprite (Cu_2O) and the redness of the metallic surface. Sulphate-based pollutants promote the formation of

*Correspondence: henri.schrekker@ufrgs.br
[1] Laboratory of Technological Processes and Catalysis, Institute of Chemistry, Universidade Federal do Rio Grande do Sul (UFRGS), Av. Bento Gonçalves 9500, Porto Alegre, RS 91501-970,, Brazil
Full list of author information is available at the end of the article

basic sulphates such as brochantite $CuSO_4{\cdot}3Cu(OH)_3$ or $Cu_4SO_4{\cdot}(OH)_6$. Carbon dioxide and water, produce copper carbonate such as malachite $Cu_2(OH)_2CO_3$ and azurite $Cu_3(OH)_2(CO_3)_2$ [3].

Nowadays, organic coatings represent one of the most widespread approaches for the protection of metal substrates [7]. In the protection of bronze artworks, smart organic coatings have been widely proposed as a suitable approach for the inhibition of metal corrosion [8]. Such systems are characterized by a twofold protective action, as they are able to avoid the direct interaction of the metal surface with pollutants coming from the environment (passive protective mechanism) and to slow down degradation kinetics due to anticorrosive molecules that are released at the metal/coating interface and can there interfere with the chemical degradation of metal (active protective mechanism). Nonetheless, protective coatings that are suitable for artistic objects should also meet some specific requirements such as transparency, long-term efficiency and reversibility or, at least, reapplicability. Generally, the commonly used commercial products are based on acrylic resins or microcrystalline waxes dispersed in harmful solvents such as toluene and white spirit. Some notable examples include Incralac®, which consists of Paraloid B44™, a copolymer of methyl methacrylate with an undefined monomer, dispersed in toluene, and Soter, microcrystalline waxes dispersed in a turpentine and ether mixture. Often these products are combined in double-layer systems to enhance their protective actions (such as Incralac® and wax) [9]. Fluoropolymers have also been used because of their high resistance to ultraviolet exposure degradation [10]. Alternatively, safer coatings consisting of renewable polysaccharides such as chitosan (CHT) [11], benzotriazole (BTA) end-capped poly(lactic acid)s [12] as well as hybrids coatings consisting of siloxane domains embedded in polymeric phases [13] have been recently investigated. In this context, some of the authors of the present work have recently exhaustively investigated the potentials of water-based active coatings based on CHT [14] or high amorphous polyvinyl alcohol with mercaptobenzothiazole loaded layered double hydroxide nanoparticles [15] as suitable coatings to protect bronze surfaces in an indoor environment.

BTA is the main corrosion inhibitor agent that is widely used for the protection of works of art made of copper-based alloys [16–18]. The effectiveness of BTA molecules relies on their capability to strongly form by chemisorption a two-dimensional barrier film of less than 50 angstroms, which protects copper and its alloys in aqueous media and various aggressive environments [19]. Despite this, BTA is considered as a toxic and hazard compound. Thus, great efforts are focused to limit the drawbacks related to the use of BTA. A possible solution is its immobilization within a polymer matrix such as poly(lactic acid), avoiding the leakage of such toxic agent [12]. When using CHT as polymeric matrix with embedded BTA, a synergic effect between these components improves the inhibitor efficacy, enabling to work with lower BTA contents [14]. Recently, the interest for the identification of alternative solutions has received an increasing attention and several studies have been addressed to the use of less harmful compounds, such as mercaptobenzothiazole [15, 20, 21], sodium oleate [22], 2-mercaptobenzoxazole [23], tolyltriazole [24], and cysteine [25].

In this context, imidazolium salts (IS), including ionic liquids that are IS with a melting point of 100 °C or lower, possess favorable characteristics for their application in formulations for protective coatings, e.g. negligible vapor pressure, chemical and thermal stability and low flammability [26, 27]. Generally, they consist of an imidazolium cation and an organic or inorganic anion, and their properties can be tuned by structural changes in the ions, enabling the preparation of task-specific ionic liquids [28]. Besides, their negligible vapor pressures turns them into ideal candidates to minimize the risk of inhalation. In this perspective, BTA-functionalized imidazolium ionic liquids have been synthesized as effective corrosion inhibitors for steel and copper [29]. Their corrosion inhibition mechanism is similar to what is known for most of the organic corrosion inhibitors, blocking the anodic and cathodic reactive sites on a metallic surface through: (a) electrostatic adsorption of IS ions on anodic and cathodic surface sites; (b) chemisorption; and (c) surface interactions between IS compounds, forming a 2D barrier coating [30, 31].

The present work fits in this frame; focused on the use of IS to improve the performances of CHT-based coatings intended for the protection of bronze surfaces. More specifically, we investigated the potential of the carboxyl-functionalized IS 1-carboxymethyl-3-methylimidazolium bis (trifluoromethylsulfonyl) imide (**$HO_2CC_1MImNTf_2$**; Fig. 1) as additive in CHT-based coatings for the

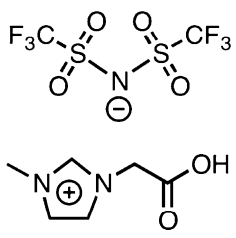

Fig. 1 Imidazolium salt explored in this study

exploitation of several roles: (a) anticorrosion additive; and (b) co-anticorrosion additive in the presence of BTA.

In particular, **$HO_2CC_1MImNTf_2$** was selected for the development of coating formulations, showing benefits over the IS presented in Fig. 2. The application of coatings with hydrophobic IS (Fig. 2a) protected the alloy only in the areas covered with IS. Most likely the incompatibility between the hydrophobic IS and the hydrophilic CHT caused the presence of uncovered areas. Similarly, BTA-functionalized IS (Fig. 2b) did not afford the desired protection due to their low solubility's in water:ethanol (50:50), which was used to solubilize CHT. Within the screened hydrophilic IS (Figs. 1 and 2c), which are soluble in water:ethanol (50:50), **$HO_2CC_1MImNTf_2$** was the most promising IS. The optimum **$HO_2CC_1MImNTf_2$** content was chosen to be 35 wt% with respect to the CHT content. Besides, 2 wt% of BTA, with respect to the CHT content, was selected, being comparable with the amount typically used in commercial products.

The protective efficacy of the investigated IS formulations was evaluated by submitting coated bronze disks to an accelerated test in acidic conditions. In order to promote the corrosion processes at the alloy surface, the disks were treated with acidic water vapors containing chloride ions by using a procedure previously reported [14, 15, 32–34]. The degradation processes in bronze objects are very complex and can be induced by several species. Therefore, chloride ions were selected to perform the tests since they are among the most aggressive degrading agents for copper-based alloys. In this way, it was possible to rapidly obtain information about the protective efficacy of the investigated formulations.

A copper-based alloy, with chemical composition and dendritic metallurgical structure similar to those commonly used in bronze objects of art, was used as the metallic substrate. In this work the comprehensive results related to the morphological, chemical and functional characterization of the best CHT-based coatings modified with BTA, **$HO_2CC_1MImNTf_2$** and the mixture BTA- **$HO_2CC_1MImNTf_2$** are reported. The results confirm that the selected IS, **$HO_2CC_1MImNTf_2$**, does not affect the esthetical characteristics of pristine CHT-based coating and, when used at 35 wt% with respect to CHT and in the presence of 2 wt% of BTA, has a positive effect on the anticorrosion effectiveness of the resulting coating when compared to the CHT system containing only 2 wt% of BTA. This result is likely ascribed to an improvement of interfacial adhesion between the CHT matrix and the metal substrate. To the best of our knowledge, this preliminary study on the active protection of bronze alloys with CHT-based coatings modified with BTA and the IS **$HO_2CC_1MImNTf_2$** is innovative and similar uses of IS in cultural heritage were not reported so far.

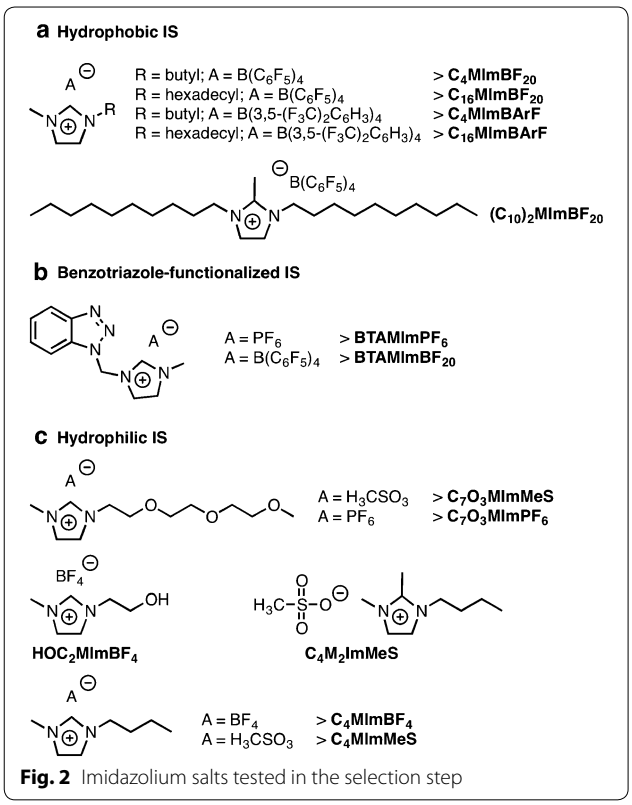

Fig. 2 Imidazolium salts tested in the selection step

Experimental

Materials

1-Methylimidazole (99%), methyl 2-chloroacetate (99%), lithium bis (trifluoromethylsulfonyl) imide ($LiNTf_2$, 99.95%), dichloromethane (P.A.), magnesium sulfate (≥ 99.5%), silver nitrate (99.5%), CHT (medium molecular weight, viscosity 200–800 cP, 75–85% deacetylated), D-(+)-gluconic δ-lactone (DGL, ≥ 99.9%), ethanol (≥ 99.8%), water Cromasolv plus for HPLC, hydrochloric acid (37%, ACS reagent) and sodium hydroxide (≥ 97.0%, pellets, ACS reagent) were purchased from Sigma-Aldrich. BTA (99%) was purchased from Bresciani. Glacial acetic acid (99.9%) was purchased from Carlo Erba. Before using, CHT was washed in boiling water for 1 h, filtered, thoroughly washed with distilled water to remove impurities, and dried under vacuum for 12 h.

Bronze substrate

A copper-based alloy with nominal composition of 85 wt% Cu, 5 wt% Sn, 5 wt% Pb, and 5 wt% Zn, produced by casting and with a dendritic structure, was used as representative metal substrate [3]. The alloy disks have been polished by using SiC papers at 1200 grit and, subsequently, diamond pastes up to 1/4 µm. After polishing, the Cu-based alloy disks were cleaned with ethanol.

Atomic force microscopy (AFM)

Surface roughness was measured with a Dimension 3100 atomic force microscope, equipped with a NanoScopeIV controller (Veeco, Santa Barbara, CA), operating in tapping mode. Phosphorus-doped silicon probes with a resonant frequency of around 275 kHz and a nominal spring constant of 20/80 Nm were employed (RTESP) (Veeco, Santa Barbara, CA). A scan rate of 0.2 Hz was employed at a resolution of 384 pixels/line. The root mean square roughness of polished bronze substrate was determined in a scan area of $50 \times 50\ \mu m^2$.

Synthesis of 1-carboxymethyl-3-methylimidazolium bis (trifluoromethylsulfonyl) imide ($HO_2CC_1MImNTf_2$)

Scheme 1 shows the synthetic route that was applied for the preparation of $HO_2CC_1MImNTf_2$. Initially, a literature procedure was used for the synthesis of 1-carboxymethyl-3-methylimidazolium chloride (HO_2CC_1MImCl) [35]. A bimolecular nucleophilic substitution reaction (SN_2) between 1-methylimidazole (2.02 g, 24.6 mmol, 1.00 equiv.) and methyl 2-chloroacetate (2.30 g, 24.6 mmol, 1.00 equiv.) was performed for 1 h at 0 °C to prepare the ester-functionalized IS 1-methoxycarbonylmethyl-3-methylimidazolium chloride ($H_3CO_2CC_1MImCl$). Subsequently, this IS was treated with HCl (24.6 mmol, 1.00 equiv.) for 3 h at 100 °C to synthesize HO_2CC_1MImCl.

A literature procedure was used for the anion metathesis [36]. HO_2CC_1MImCl (0.503 g, 2.85 mmol, 1.00 equiv.), $LiNTf_2$ (0.858 g, 2.99 mmol, 1.05 equiv.) and water (25.0 mL) were mixed and stirred at room temperature (rt) for 24 h. This solution was extracted with dichloromethane (3×35 mL), and the joined organic phase was dried over magnesium sulfate. Filtration followed by solvent evaporation afforded $HO_2CC_1MImNTf_2$.

Nuclear magnetic resonance (NMR)

NMR spectra of HO_2CC_1MImCl and $HO_2CC_1MImNTf_2$ were recorded on Bruker (400 MHz) and Varian Inova (300 MHz) spectrometers at ambient temperature. The chemical shifts are given in parts per million (ppm) and referenced to the residual solvent signal ($D_2O = 4.79$ (^1H); dimethyl sulfoxide-d6 = 39.52 (^{13}C)).

Mass spectrometry-Electrospray ionization (MS–ESI)

The MS–ESI spectrum of $HO_2CC_1MImNTf_2$ was recorded on an electrospray ionization (ESI) Q-Tof Micro™ equipment (Micromass, Manchester, UK) in the positive mode.

In vitro cytotoxicity of $HO_2CC_1MImNTf_2$ and BTA

For the cytotoxicity tests, IS and BTA were washed several times with phosphate buffer solution and freeze dried to obtain dry powders. Then, IS and BTA solutions in Dulbecco's modified Eagle's medium (GIBCO® by Life Technologies, Italy) at concentrations of 10, 100, 200, 350 and 500 μg mL^{-1} were prepared in an incubator shaker at 37 °C for 3 h, and then sterilized for 2 h under ultraviolet

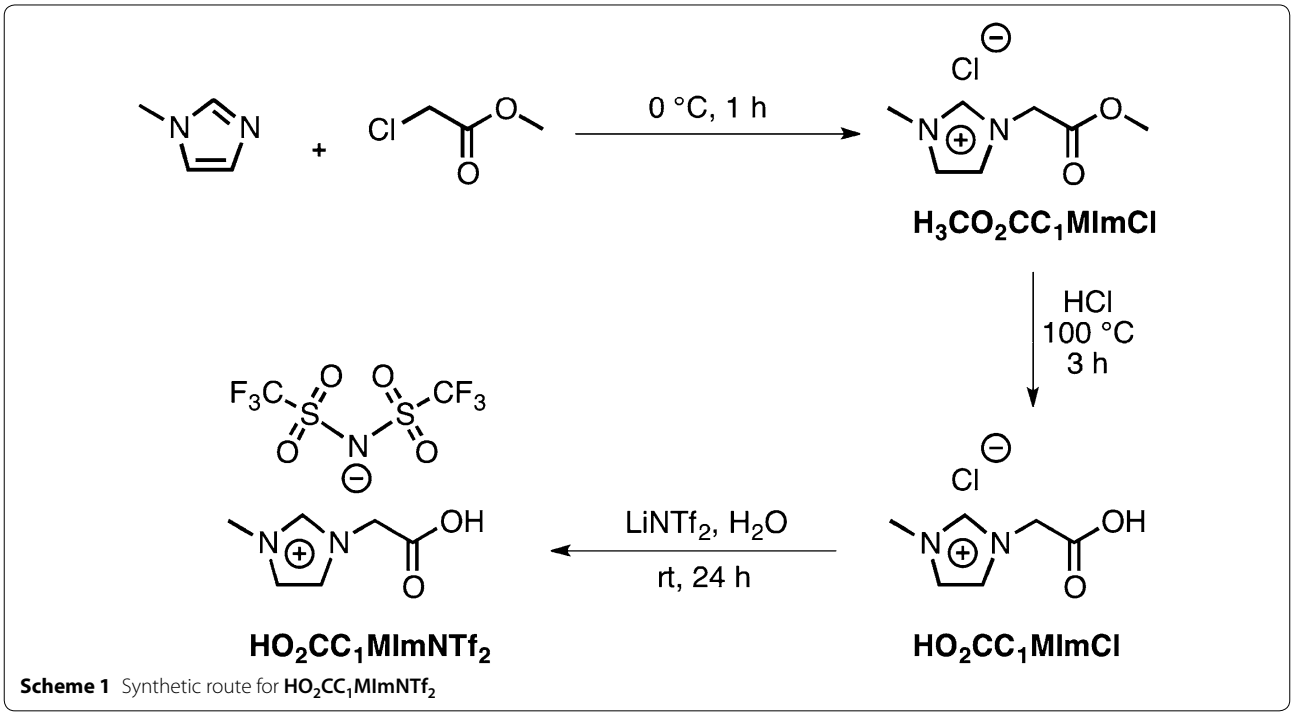

Scheme 1 Synthetic route for $HO_2CC_1MImNTf_2$

radiation ($280 < \lambda < 200$). The wells of Falcon® 48-well culture plates were seeded with 5000 cells (50 µL) of 80% confluent mouse fibroblast (L929) cell line (in accordance with the standard international guideline ISO10993-5), followed by the addition of 350 µL of a chosen IS or BTA solution. Dulbecco's modified Eagle's medium without IS and BTA was used as negative (non-toxic) control. The incubation was performed at 37 °C (5% CO_2, 97% air humidity) for 1 and 5 days of exposure. Alamar Blue (Invitrogen, Italy) was used as a redox indicator to evaluate biocompatibility. This assay quantified the redox indicator that changed to a fluorescent product in response to chemical reduction by mitochondrial enzymes such as dinucleotide adenine flavin dehydrogenase and dinucleotide adenine nicotinamide dehydrogenase, providing a quantifiable indication for the metabolic activity of living cells. After the selected times of 1 and 5 days, the medium was removed and a 200 µL aliquot of diluted Alamar Blue (1:10) in red phenol-free medium (GIBCO® by Life Technologies, Italy) was added to each well. After incubation for 4 h at 37 °C (5% CO_2, 97% air humidity), 100 µL of each solution was transferred to a 96-well plate for colorimetric analysis (n = 4). Wells without any cells were used to correct any background interference of the redox indicator. Cell viability was correlated with the magnitude of the dye reduction and expressed as % AB reduction according to the manufacturer's protocol.

Preparation of chitosan-based coatings and characterization

The pure CHT formulation (**CHT**) was prepared by adding the CHT powder (1.0 wt%/vol%) to an aqueous DGL solution (0.05 M) and then the mixture was kept under stirring for 24–30 h to achieve complete solubilization of the polymer. The final pH of the solution was adjusted to 6 by the addition of 1 M sodium hydroxide solution. The corrosion inhibitor BTA (2.0 wt% with respect to CHT) was added to the CHT suspension from DGL (pH = 6) to prepare the formulation **CHT/BTA**. The formulation **CHT/IS** was prepared by dissolving 35 wt% (with respect to CHT) of $\mathbf{HO_2CC_1MImNTf_2}$ in the water/ethanol CHT solution from DGL (pH = 6). The **CHT/BTA-IS** formulation was prepared by adding both BTA (2.0 wt% with respect to CHT) and $\mathbf{HO_2CC_1MImNTf_2}$ (35 wt% with respect to CHT) to the pure CHT solution from DGL (pH = 6). All the solutions were diluted with ethanol to obtain formulations with a final water/ethanol composition of 50/50 vol%/vol%. The coatings were prepared by solvent casting, dropping 320 µL of the water/ethanol CHT-based formulations on the reference bronze disks with a diameter of 30 mm and subsequent drying overnight at rt.

Colorimetric analysis

Color differences between an uncoated copper-based alloy disk and disks coated with **CHT**, **CHT/BTA**, **CHT/IS**, or **CHT/BTA-IS** were measured with an Exact color spectrophotometer (X-Rite, Grand Rapids, MI, USA). Color differences in the CIELab space were evaluated by using the uncoated copper disk as a reference and measuring the ΔL*, Δa* and Δb* values, where L* is the color lightness, a* is the green-magenta contribution and b* is the blue-yellow contribution. For each sample, three colorimetric measurements were performed and average values of ΔL*, Δa*, and Δb* were obtained. For each couple of specimens, the Euclidean difference ΔE* was calculated using Eq. 1 [37]:

$$\Delta E = \sqrt{(\Delta L^*)^2 + (\Delta a^*)^2 + (\Delta b^*)^2} \quad (1)$$

Nanoscratch test

The nanoscratch test was performed to investigate the abrasion resistance of the coatings. The experiments were carried out with a NanoTest Platform made by Micro Materials Ltd., equipped with a Berkovich diamond tip of three-side pyramidal geometry. In a typical experiment, the indenter tip was moved tangentially over the coating surface at a fixed velocity of 1 µm s^{-1} while progressively increasing the applied normal load up to 50 mN over a scratch length of 2 mm.

Accelerated corrosion test

In order to assess the protective efficacy of the CHT-based coatings, accelerated corrosion tests were carried out by heating the coated bronze disks inside a closed glass vessel at 50 °C in the presence of HCl vapor (aqueous 1.0 M HCl solution) and 100% relative humidity (RH). Note that bronze disks were exposed to acid vapor but not in direct contact with the HCl solution (Fig. 3).

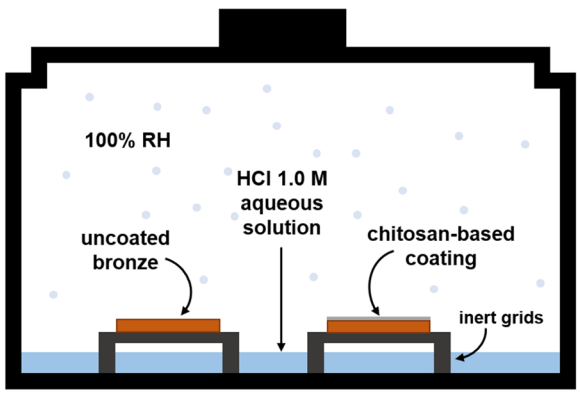

Fig. 3 Treatment environment for accelerated corrosion of bronze under a HCl atmosphere

The coated bronze disks were characterized before and after the test at different time intervals (up to 12 h). All the characterizations were conducted in the central part of the disks where the border effect is not relevant. After the corrosion treatment, the CHT-based films were partially removed by using tissue paper soaked in water and ethanol.

Optical microscopy (OM) and image analysis

For the evaluation of the protective efficacy of the coatings, modifications at the metal surface were analyzed by means of OM. The investigations were carried out with a Leica MEF 4 M microscope equipped with a digital camera (Leica DFC 280). Image analysis has been exploited to characterize the state of the metal surface after the accelerated corrosion test. OM images at the metal/coating interface were collected without removing the coating, and the percentage of corroded surface was estimated through a custom-tailored image analysis protocol, whose details can be found elsewhere [14, 15]. Briefly, OM images were first equalized and converted into grayscale, in which lighter tones correspond to not corroded areas, while darker ones to corroded areas. Then, a threshold tone distinguishing corroded and not corroded areas was arbitrary and uniquely defined. Finally, the percentage of corroded area was estimated from the histograms corresponding to the relative frequency of the tones extracted from each grayscale image. Images of untreated coated disk were used as reference.

Attenuated total reflectance–Fourier transform infrared (ATR–FTIR) spectroscopy

Bronze disks with CHT-based coatings containing BTA and/or **$HO_2CC_1MImNTf_2$** were characterized before and after the accelerated corrosion test by ATR–FTIR spectroscopy. This was performed with the aid of a Nicolet iS50 spectrometer (Thermo Fisher Scientific). The samples were characterized by forcing their coated surface in contact with the diamond crystal and taking care that the pressure was constant for all analyses. The spectra were collected by 32 scans at a resolution of 4 cm^{-1}. All the spectra were then normalized with respect to the peak a 1583 cm^{-1}, which can be ascribed to the N–H bending of the CHT primary amine groups and the DGL used for the CHT solubilisation in water [14, 38]. No ATR correction has been applied to the data.

Scanning electron microscopy (SEM) analysis

The determination of the thickness (before and after the corrosion test), and micro-chemical and -morphological characterisations of the coatings (before and after the corrosion test) were performed by means of a scanning electron microscope Cambridge 360 equipped with a LaB6 filament and a high brilliance LEO 1530 field emission scanning electron microscope apparatus equipped with an energy dispersive X-ray spectrometer (EDS).

Results and discussion

HO_2CC_1MImCl (Scheme 1) was obtained as white solid and the two-step synthesis resulted in 92% yield. The recorded ^1H (Additional file 1: Figure S1) and ^{13}C NMR (Additional file 1: Figure S2) spectra are in agreement with the data published previously [35]. As chloride anions promote the bronze disease, anion methatesis between chloride and bis (trifluoromethylsulfonyl) imide was performed (Scheme 1). This reaction resulted in the formation of **$HO_2CC_1MImNTf_2$** as transparent oil in 38% yield. A test with acidified silver nitrate indicated the absence of chloride. The ^1H (Additional file 1: Figure S3) and ^{13}C NMR (Additional file 1: Figure S4) spectra correspond to the chemical structure of **$HO_2CC_1MImNTf_2$**. When considering the ^1H NMR data (300 MHz, D_2O): δ (ppm) 8.74 (s, 1H, C2-H), 7.45–7.44 (m, 2H, C4-H and C5-H), 5.02 (s, 2H, CH_2), 3.89 (s, 3H, CH_3); the number of peaks and their corresponding integrals verify the chemical identity of **$HO_2CC_1MImNTf_2$**. The same counts for the ^{13}C NMR data (100 MHz, dimethyl sulfoxide-d6): δ (ppm) 169.8 (CO_2H), 136.7 (C2), 122.9 (C4/5), 122.8 (C5/4), 118.6 (qua, $J = 319.7$ Hz, CF_3), 49.6 (CH_2), 35.2 (CH_3). MS-ESI(+) detected m/z 141.1201 for the cation of **$HO_2CC_1MImNTf_2$**, which is close to the calculated value of 141.0659 for $C_6H_9N_2O_2^+$.

For **$HO_2CC_1MImNTf_2$** and BTA, their cytotoxicity were determined in cells from the mouse fibroblast cell line (Fig. 4). Compared to the cell proliferation of the control (IS- and BTA-free), **$HO_2CC_1MImNTf_2$** showed similar cell viability after 1 day, independent of the applied IS concentration. After 5 days, the cell proliferation in the presence of **$HO_2CC_1MImNTf_2$** was without significant difference compared to the control or about 30% lower for the samples at 200 and 500 μg mL^{-1} (Fig. 4a). Overall, the obtained cytotoxicity data on in vitro murine fibroblast cells indicated no cytotoxic effect of **$HO_2CC_1MImNTf_2$** and the safe use of this IS in the protective formulations as demonstrated by the capability of **$HO_2CC_1MImNTf_2$** to support increasing cell proliferations over the culture time. BTA showed a different profile in this cytotoxicity assay (Fig. 4b). Now, the cytotoxicity increased with increasing BTA concentrations. At the lower concentrations of 10 and 100 μg/mL, although BTA was not toxic after 1 day, a significant reduction in cell proliferation (about 50% compared to the control) was observed at day 5, where the toxic effect was evident. These results confirm that **$HO_2CC_1MImNTf_2$** is less cytotoxic than BTA, which is an important insight

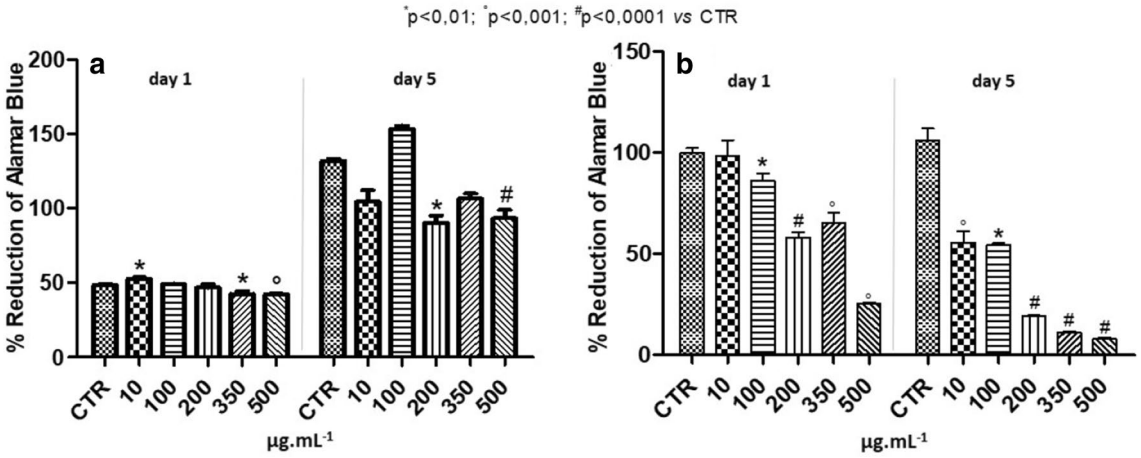

Fig. 4 Cytotoxicity of **a** $HO_2CC_1MImNTf_2$ and **b** BTA against L929 mouse fibroblast cells, after 1 day and 5 days (CTR = control = IS- and BTA-free)

that justifies the strategic selection made in this paper to address the research towards more sustainable anticorrosive compounds as compared with traditional BTA.

To assess the efficacy of the CHT-based coatings functionalized with the IS $\mathbf{HO_2CC_1MImNTf_2}$ and/or BTA, a copper-based alloy was used as metal model substrate. The alloy disks were polished to obtain a flat and smooth surface with a mirror-like finish. Surface analysis by AFM enabled the determination of the root mean square roughness, being 17.7 ± 4.31 nm. The preparation of CHT-based formulations was optimized to obtain uniform, compact and transparent films after deposition on Cu-based disks and drying. In particular, DGL was used to solubilize the polymer and an ethanol/water mixture with composition of 50/50 vol%/vol% was selected as liquid medium (formulation **CHT**). The commonly used corrosion inhibitor BTA (2 wt% with respect to CHT; formulation **CHT/BTA**), the IS $\mathbf{HO_2CC_1MImNTf_2}$ (35 wt% with respect to CHT; formulation **CHT/IS**) and the mixture of BTA and $\mathbf{HO_2CC_1MImNTf_2}$ (2 and 35 wt% with respect to CHT, respectively; formulation **CHT/BTA-IS**) were added to the **CHT** formulation and investigated as protective agents.

The colour coordinates for the different samples and the ΔE* values calculated with respect to the pristine bronze disk are reported in Table 1. Colorimetric analysis in the CIELab space revealed that the coatings present a very small impact on the aesthetic appearance of the original bronze substrate. The ΔE* values, indeed, are small and compatible for applications in cultural heritage, which is ΔE* below the threshold of 5, being considered the lower limit for human eye perception [39, 40]. The only exception is represented by the coating obtained from the formulation **CHT/BTA**, which presented a significant variation with respect to the pristine bronze disk (i.e. $\Delta E^* > 5$). Looking at the color coordinates, it emerges that the largest variation with respect to the uncoated bronze surface was found for the L* value (variation of −38%). This indicated that the presence of the **CHT/BTA** coating caused a significant reduction of the color lightness of the metal substrate, probably due to a poor dispersion of BTA in the chitosan matrix and/or the formation of small BTA crystalline precipitates. At the same time, we highlight that the coating containing both the IS and the corrosion inhibitor (**CHT/BTA-IS**) exhibited the lowest ΔE* among the coatings with additives, its value being very similar to that related to the **CHT** coating. This suggested a synergic effect between IS and BTA in not affecting the appearance of the metal surface. In this sense, it is worth noting that the ΔE* values of the coatings developed in the present work, and in particular that of the **CHT/BTA-IS** coating, are much lower than other values reported in the literature for BTA-containing protective coatings for bronze surfaces [41].

Table 1 The color coordinates for the bronze disks coated with chitosan-based formulations

	L*	a*	b*	ΔE*
Bronze	13.56	7.52	20.03	–
CHT	12.28	7.68	20.29	1.3
CHT/BTA	8.39	8.79	22.17	5.7
CHT/IS	10.93	9.21	21.19	3.3
CHT/BTA-IS	11.98	7.24	20.64	1.7

Figure 5 shows the ATR–FTIR transmittance spectra of the prepared coatings on bronze disks. The spectrum of the **CHT** coating exhibits the typical peaks of DGL

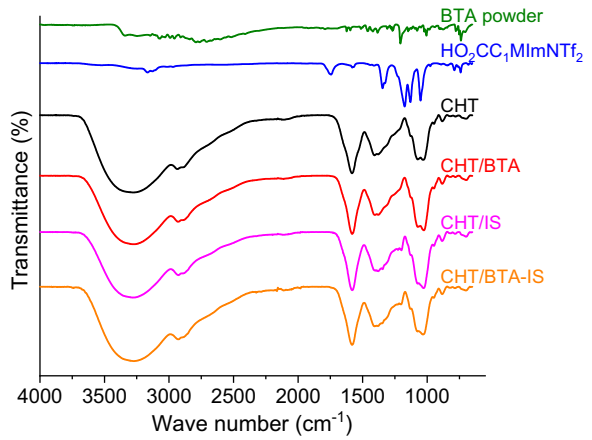

Fig. 5 ATR–FTIR spectra of the **CHT**, **CHT/BTA**, **CHT/IS**, and **CHT/BTA-IS** coatings deposited on bronze disks. The spectra of pristine BTA and **$HO_2CC_1MImNTf_2$** are also given as reference

and CHT polymer according to the assignments already reported [14]. In the case of **CHT/BTA**, the BTA content of 2 wt% with respect to the amount of polymer was to low to be detected in the spectrum. On the other side, the presence of IS **$HO_2CC_1MImNTf_2$** at 35 wt% with respect to the amount of polymer was clearly evidenced in the spectrum of **CHT/IS** by three transmittance peaks in the range of 1400–1100 cm^{-1}. It is worth noting that one of these peaks is clearly observed in the spectrum of pristine **$HO_2CC_1MImNTf_2$** at 1358 cm^{-1} and may be ascribed to C–N (stretching vibration) bands in imidazolium rings [42]. The other two peaks at around 1220–1230 cm^{-1} may tentatively be ascribed to intimate CHT-IS interactions. Part of the CHT amines is protonated (being solubilized in acidic conditions), which may interact with the IS anion, bis (trifluoromethylsulfonyl) imide.

The coating thickness measured by SEM was about 8–14 µm for all the investigated samples (Additional file 1: Figure S5). SEM micrographs showed that the surfaces were homogeneous without apparent cracks or domains due to separations of components. A representative SEM micrograph is reported in Fig. 6, showing in the right part the surface coated with **CHT/BTA-IS** and in the left part the bare surface of bronze disk after removal of this coating. The EDS spectra confirmed the effective removal of the coating (Fig. 6). At higher magnification, the surface of the coating appears without any cracks and any phase separation confirming that all components of the coating are fully miscible in the composition range investigated.

A representative output of the progressive-load nanoscratch measurements is given in Fig. 7, showing both the optical micrographs of the scratch paths and the initial parts of the nanoscratch profile curves, which enabled determining the coating failure.

Nanoscratch tests offer the possibility of assessing the quality of the coating/substrate interactions. This can be done by looking at the coating failure mode during/after scratch and also by comparing the depth vs. load curves

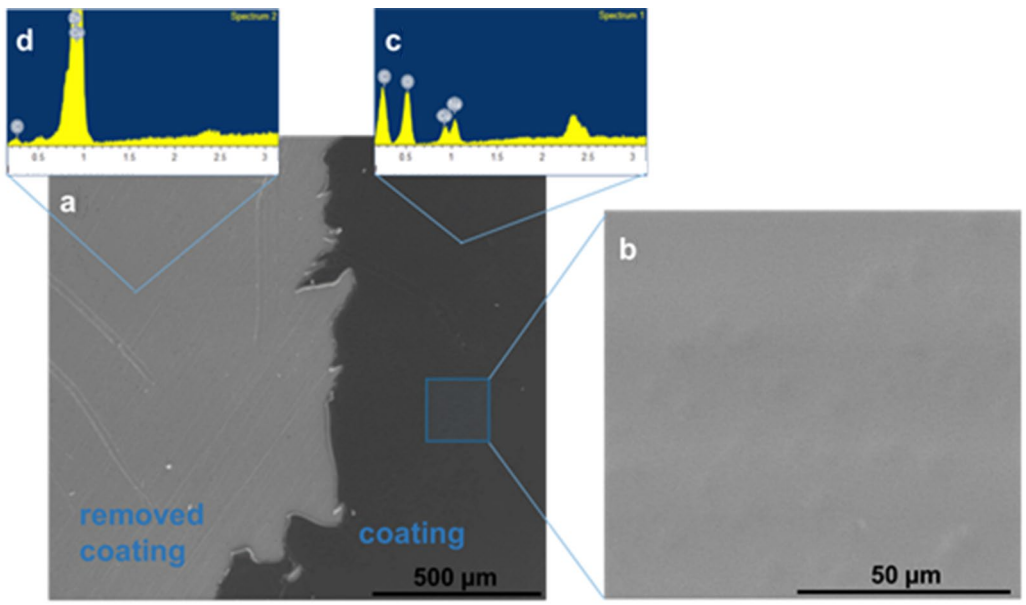

Fig. 6 **a** Representative SEM micrograph (scale bar = 500 µm) of the bronze disk covered with **CHT/BTA-IS** (right: darker area) and after removal of this coating (left: brighter area). **b** Magnification of the part coated with **CHT/BTA-IS** (scale bar = 50 µm). **c**, **d** EDS spectra of both parts are also shown

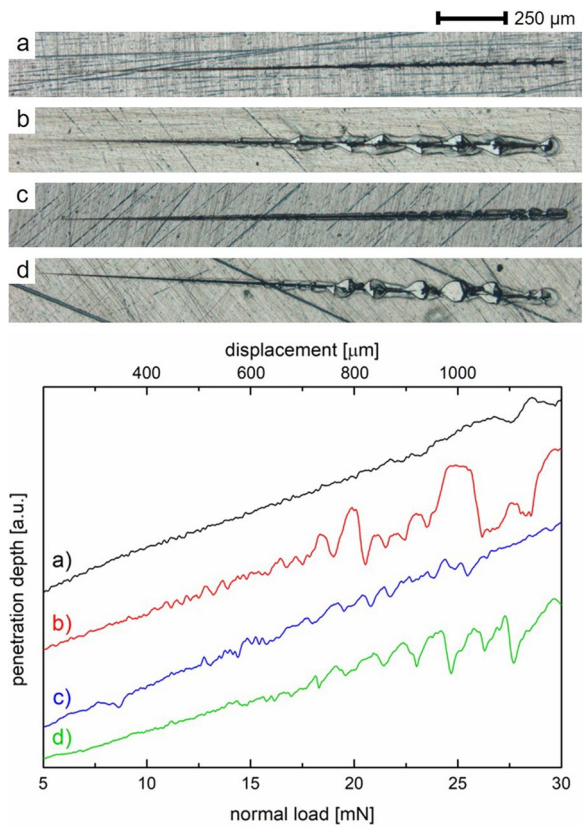

Fig. 7 Representative optical micrographs of the scratch paths for **a CHT**, **b CHT/BTA**, **c CHT/IS** and **d CHT/BTA-IS** coatings on bronze disks. The corresponding initial part of the nanoscratch curves (applied normal load between 5 and 30 mN) is also given for the same coatings; the curves have been vertically shifted for the sake of clarity

recorded during the scratch [43]. The analysis of the optical micrographs of the scratch paths in Fig. 7 highlights that a modest deformation occurred for relatively low loads for all the coatings. On the contrary, at higher loads the formation of pile-up material on either side of the track becomes significant, the effect being much more pronounced in the case of samples containing BTA. The latter presumably plasticizes the polymer matrix [14], which on the contrary showed a very good adhesion to the metal surface. More specifically, when the coating/substrate adhesion is poor, a significant amount of coating material is generally stripped of along the entire length of the scratch path [44]. This is the case of the **CHT/BTA** sample. On the contrary, the addition of the IS only slightly affected the already good chitosan-bronze adhesion, as indicated by the similarity of the scratch paths of pristine polymer (**CHT**) and polymer with IS (**CHT/IS**). From a practical perspective, a comparative evaluation of the coatings can be done in terms of critical scratch load, which is the load value at which the coating fails [45]. In this sense, the **CHT** coating exhibited the best performances, followed by **CHT/IS**, **CHT/BTA-IS**, and **CHT/BTA**. This rank is further supported by the profiles of the scratch curves, especially when looking at their initial part (i.e. up to 30 mN of applied load). Besides the different slope, which is mainly related to the different grade of flatness of the bronze substrates, the curves in Fig. 7 are clearly rougher for the samples containing BTA (both **CHT/BTA** and **CHT/BTA-IS**). This indicates that its addition caused a lowering of the abrasion resistance of the CHT matrix and decreased the adhesion of the coating to the underlying metal surface. Nonetheless, a closer look at the curves also suggests that the presence of the IS in **CHT/BTA-IS** helped in partially recovering the good adhesion to the substrate and high scratch resistance of the pristine CHT coating. This behaviour can be possibly ascribed to the electrostatic interactions that took place between the metal cations present on the bronze surface and the IS bis (trifluoromethylsulfonyl) imide anions (Fig. 1), abbreviated as NTf_2:

$$M^{n+} + n\left(NTf_2^-\right) \rightarrow M^{n+} \ldots n\left(NTf_2^-\right)ads$$

Due to this interaction, the positively charged CHT matrix (rich of ammonium ions due to the solubilisation performed in acidic conditions) may strongly compete with the imidazolium cations of the IS to interact with the functionalized substrate. As a consequence, the polymer forms a continuous film that protects the substrate and increases the adhesion to the metal of the modified film:

$$M^{n+} \ldots n\left(NTf_2^-\right)ads + Chit^{n+} \rightarrow M^{n+} \ldots n\left(NTf_2^-\right)ads \ldots Chit^{n+}$$

Although further investigations are necessary, a similar mechanism was recently considered to explain the protective effect of dicationic IS on steel substrates in acidic conditions [46].

With the aim to investigate the protective efficacy of the developed coatings, all the coated disks were subjected to accelerated corrosion treatments and the occurrence of surface modifications was observed at different time intervals by optical microscopy.

In the case of the coatings **CHT** and **CHT/IS**, significant modifications of the alloy surface were observed after 6 h of accelerated corrosion test (Fig. 8).

These results suggest that the **CHT** and **CHT/IS** coatings were not stable and able to prevent the occurrence of corrosion processes under the tested conditions. The hypothesis of the coating degradation was supported by ATR–FTIR analysis since the small peak at 880 cm^{-1}, typical of the wagging (the CH bending out of plane of the saccharide ring) of the CHT structure

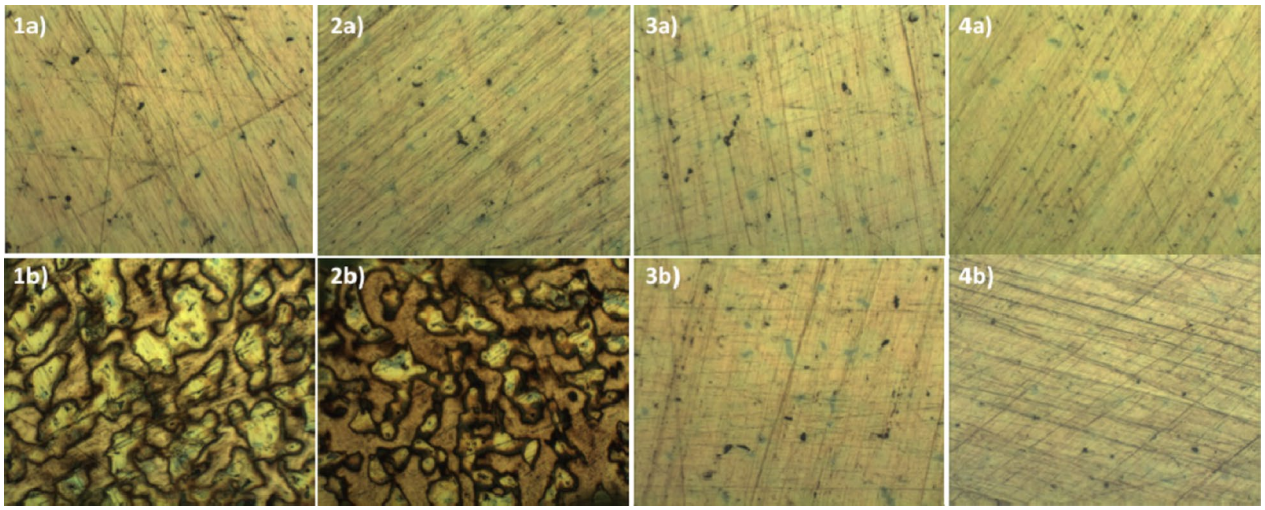

Fig. 8 Optical micrographs (magnification 100×) of bronze disks coated with **CHT** (**1**), **CHT/IS** (**2**), **CHT/BTA** (**3**) and **CHT/BTA-IS** (**4**) before (**a**) and after (**b**) exposure to HCl vapor for 6 h

[47], disappeared after the exposure to aggressive vapors. Moreover, the ATR–FTIR spectra of the **CHT** and **CHT/IS** coatings, after exposure to HCl vapors, revealed the presence of two weak bands in the region between 1000 and 800 cm^{-1}, being characteristic for the bending of the hydroxyl groups in $Cu_2(OH)_3Cl$ species. In particular, the band at 913 cm^{-1} confirmed the presence of atacamite, while the one at 863 cm^{-1} can be attributed to clinoatacamite and anatacamite. The ATR–FTIR transmittance spectra of the **CHT/IS** coating, before and after 6 h of accelerated corrosion, are reported as an example in Fig. 9.

On the contrary, no changes on the alloy substrates were observed in the case of the coatings with BTA and the BTA-IS mixture (Fig. 8). Prolonging the corrosion treatment up to 12 h, the coating **CHT/BTA-IS** was still stable and able to prevent modifications of the metal substrate, whereas in the case of the coating **CHT/BTA** significant alterations were detected on the alloy surface. Some representative optical images are reported in Fig. 10. Furthermore, the ATR–FTIR spectroscopy analysis of the coating after 12 h of exposition to the acid vapors showed the formation of basic copper chlorides corrosion products (Additional file 1: Figure S6).

The superior performance of the coating **CHT/BTA-IS** was also confirmed by ATR–FTIR spectroscopy as no changes of the chitosan structure are observed in the FTIR spectrum after exposure to the aggressive vapors for 12 h. Moreover, FTIR bands attributable to the presence of corrosion products were not detected in the spectrum of the **CHT/BTA-IS** coating after corrosion treatment (Fig. 11).

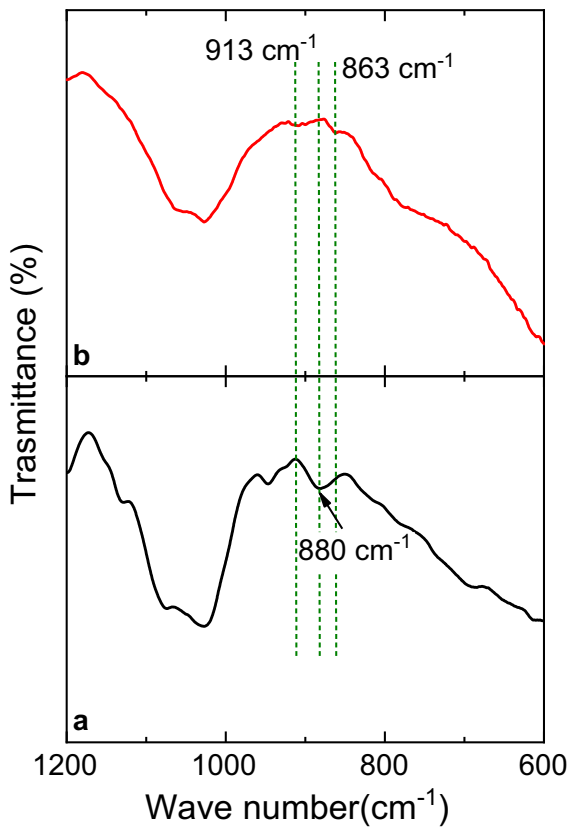

Fig. 9 ATR–FTIR spectra of **CHT/IS** coated bronze disk before (**a**) and after 6 h (**b**) of accelerated corrosion treatment

In order to get more information about the coatings and the metal surfaces after the corrosion test, the coated alloy disks were further investigated by SEM–EDS

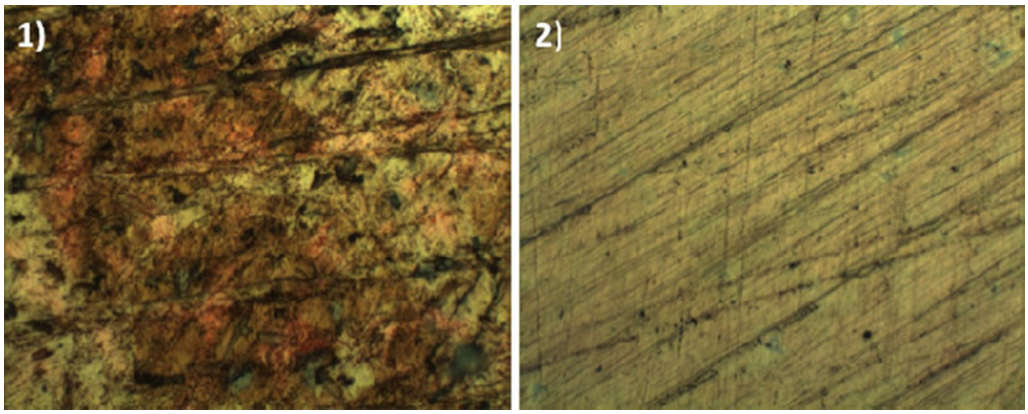

Fig. 10 Optical micrographs (magnification 100×) of bronze disks coated with the formulations **CHT/BTA** (**1**) and **CHT/BTA-IS** (**2**) after 12 h of accelerated corrosion

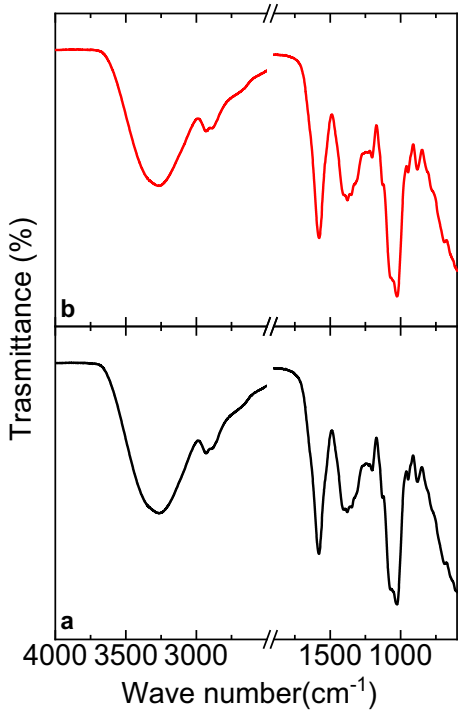

Fig. 11 ATR–FTIR spectra of **CHT/BTA-IS** coating on bronze disk before (**a**) and after 12 h (**b**) of accelerated corrosion treatment

analysis. The SEM micrographs (Fig. 12) of the coating **CHT/BTA-IS** were recorded near the area where the film was removed after the corrosion treatment. It is clearly visible that the coating was still homogeneous and crack-free even after the prolonged exposure to aggressive vapors. Moreover, the alloy surface did not show significant modifications after film removal.

On the contrary, the SEM micrographs of the **CHT/BTA** coating reveal both the alteration of the film and the formation of degradation products on the alloy substrate after film removal (Fig. 13). EDS analysis confirmed the presence of corrosion products and species containing chloride on the metal surface where the coating was removed after exposure to acid vapors (Fig. 13a, b).

In order to quantify the protective efficacy of the studied coatings, the image analysis has been performed to estimate the percentage of corroded surface, and the results are given in Fig. 14. Evidently, the pristine CHT coating **CHT** was not able to provide durable protection against corrosion, despite its very good adhesion to the bronze surface. The addition of the IS did not improve the coating protection ability, which remained essentially equal to that of the pristine CHT coating. As expected, the presence of the BTA corrosion inhibitor significantly enhanced the ability of the coating to preserve the underlying metal surface from corrosion. Actually, the presence of corrosion products at the metal/coating interface was hardly distinguishable up to 6 h of accelerated corrosion treatment. For treatments of prolonged duration, i.e. 12 h, non-negligible surface modification occurred. Interestingly, the coating containing both BTA and the IS (**CHT/BTA-IS**) provided the best corrosion inhibition, thus suggesting a synergistic effect of the two once used together. Overall, the time evolution of the percentage of corroded surface was similar to that of **CHT/BTA**. Nonetheless, it is worth noting that the amount of corroded surface was significantly lower with **CHT/BTA-IS** for longer accelerated corrosion treatments.

The obtained results show that the coating **CHT/BTA-IS** is able to protect the copper alloy surface, avoiding the formation of degradation product, even in extremely aggressive conditions. These results also suggest that $\mathbf{HO_2CC_1MImNTf_2}$ plays an important role increasing the stability and the protective properties of the **CHT/BTA** formulation.

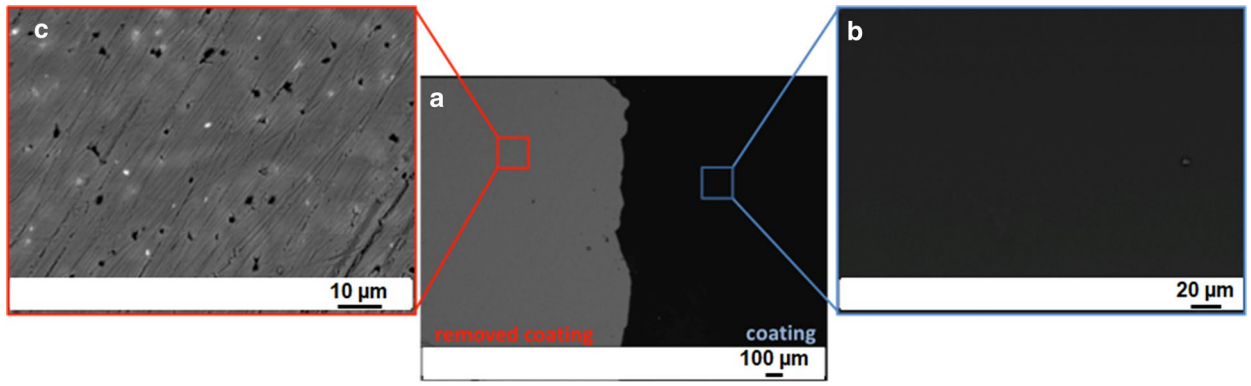

Fig. 12 SEM micrographs (different magnifications) of the boundary between the **CHT/BTA-IS** film and the alloy after 12 h of accelerated corrosion and film removal (**a**). Enlargements of the coating (**b**) and of the alloy surface after film removal (**c**)

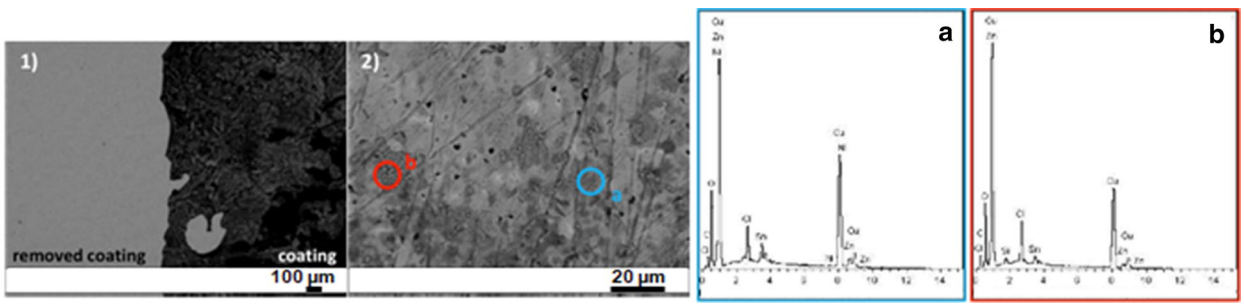

Fig. 13 SEM micrograph of the boundary between the coating **CHT/BTA** and the alloy after accelerated corrosion treatment and film removal (**1**). Enlargement (**2**) and EDS analysis (**a**, **b**) of the metal surface in the area where the coating was removed

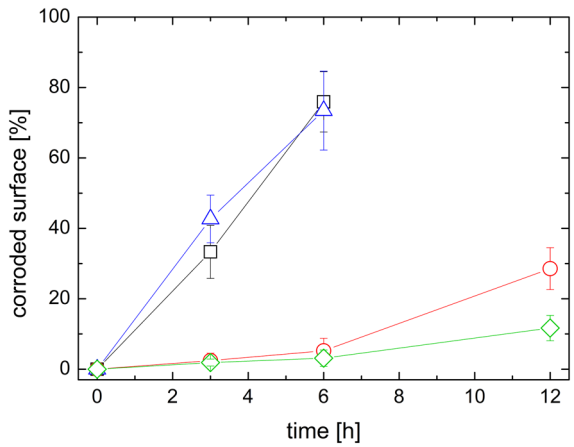

Fig. 14 Percentage of corroded surface calculated by image analysis as a function of the duration of the accelerated corrosion treatment carried out on bronze disks coated with **CHT** (black squares), **CHT/BTA** (red circles), **CHT/IS** (blue triangles) and **CHT/BTA-IS** (green diamonds)

Conclusion

In this work, IS $\mathbf{HO_2CC_1MImNTf_2}$ was investigated as potential novel corrosion inhibitor. Although this IS is less effective than BTA in the protection of bronze substrate, the use of $\mathbf{HO_2CC_1MImNTf_2}$ in combination with BTA improves the protective efficacy of the CHT-based formulation, showing a synergistic effect of the two additives. This result is of particular interest for the development of more sustainable and less toxic materials for the conservation of cultural heritage, including BTA-free coatings.

Supplementary information

Supplementary information accompanies this paper at https://doi.org/10.1186/s40494-020-00381-4.

Additional file 1. ^{1}H NMR spectra of $\mathbf{HO_2CC_1MImCl}$ (Figure S1) and $\mathbf{HO_2CC_1MImNTf_2}$ (Figure S3). ^{13}C NMR spectra of $\mathbf{HO2CC_1MImCl}$ (Figure S2) and $\mathbf{HO_2CC_1MImNTf_2}$ (Figure S4). Thickness determination by SEM for **CHT** and **CHT/BTA** (Figure S5). ATR-FTIR spectra of **CHT/BTA** coating

on bronze disk before and after 12 h of accelerated corrosion treatment (Figure S6).

Abbreviations

a*: Green–magenta contribution; AFM: Atomic force microscopy; ATR–FTIR: Attenuated total reflectance–Fourier transform infrared; b*: Blue–yellow contribution; BTA: Benzotriazole; CTR: Control; d: Doublet; DGL: D-(+)-Gluconic δ-lactone; E*: Euclidean value; EDS: Energy dispersive X-ray spectrometer; IS: Imidazolium salt(s); L*: Color lightness; m: Multiplet; MS–ESI: Mass spectrometry–electron spray ionization; NMR: Nuclear magnetic resonance; NTf_2: Bis (trifluoromethylsulfonyl) imide anion; OM: Optical microscopy; RH: Relative humidity; rt: Room temperature; s: Singlet; SEM: Scanning electron microscopy; t: Triplet; qua: Quartet; qui: Quintet; Δ: Change in a variable; **H_3CO_2C-C_1MImCl**: 1-Methoxycarbonylmethyl-3-methylimidazolium chloride; **HO_2C-C_1MImCl**: 1-Carboxymethyl-3-methylimidazolium chloride; **HO_2CC_1MImNTf$_2$**: 1-Carboxymethyl-3-methylimidazolium bis (trifluoromethylsulfonyl) imide; **CHT**: Pure chitosan coating; **CHT/BTA**: Coating of **CHT** with corrosion inhibitor BTA (2.0 wt% with respect to CHT); **CHT/IS**: Coating of **CHT** with IS **HO_2C-C_1MImNTf$_2$** (35 wt% with respect to CHT); **CHT/BTA-IS**: Coating of **CHT** with BTA (2.0 wt% with respect to CHT) and **HO_2CC_1MImNTf$_2$** (35 wt% with respect to CHT).

Acknowledgements

The authors thank Mr. Mario De Angioletti for his technical support during nanoscratch analyses, Dr. Cristina Riccucci and Dr. Marianna Pascucci for field emission SEM–EDS analyses, and Mrs. Luciana Cerri for AFM measurements.

Authors' contributions

LA, ML, GDC, MPS, TF, and HSS designed research; DKSC, KNA, MGR, CS, and CG performed research; and DKSC, EN, MSL, CG, GDC, and HSS wrote the paper. All authors read and approved the final manuscript.

Funding

This research was carried out within the framework of the NANORESTART project funded by the European Union's Horizon 2020 research and innovation program under agreement No. 646063. This study was financed in part by: the Coordenação de Aperfeiçoamento de Pessoal de Nível Superior (CAPES)-Brasil, Finance Code 001; the Conselho Nacional de Desenvolvimento Científico e Tecnológico (CNPq)-Brasil, PIBIC; and the Fundação de Amparo à Pesquisa do Estado de Rio Grande do Sul (FAPERGS)-Brasil, PROBIC.

Availability of data and materials

The datasets used and/or analyzed during the current study are available from the corresponding author on reasonable request.

Competing interests

The authors declare that they have no competing interests.

Author details

[1] Laboratory of Technological Processes and Catalysis, Institute of Chemistry, Universidade Federal do Rio Grande do Sul (UFRGS), Av. Bento Gonçalves 9500, Porto Alegre, RS 91501-970,, Brazil. [2] Institute of Polymers, Composites, & Biomaterials, National Research Council (IPCB-CNR), Viale J.F. Kennedy 54, Mostra d'Oltremare, Pad.20, 80125 Naples, Italy. [3] Institute of Polymers, Composites, & Biomaterials, National Research Council (IPCB-CNR), P.le Tecchio 1, 80055 Portici, NA, Italy. [4] Department of Chemical, Materials and Production Engineering (INSTM Consortium–UdR Naples), University of Naples Federico II, P.le Tecchio 80, 80125 Naples, Italy. [5] Institute for the Study of Nanostructured Materials, National Research Council (ISMN-CNR), Via Salaria km 29,3 Monterotondo, 00015 Rome, Italy. [6] Corrosion Laboratory, Institute of Chemistry, Graduate Program in Mining, Metallurgical and Materials Engineering (PPGE3M), Universidade Federal do Rio Grande do Sul (UFRGS), Av. Bento Gonçalves 9500, Porto Alegre, RS 91501-970,, Brazil.

Received: 3 February 2020 Accepted: 7 April 2020
Published online: 22 April 2020

References

1. Kosec T, Otma H. Investigation of the corrosion protection of chemically and electrochemically formed Patinas on recent bronze. Electrochim Acta. 2010;56:722–31.
2. Ingo GM, Riccucci C, Guida G, Albini M, Giuliani C, Di Carlo G. Rebuilding of the burial environment from the chemical biography of archeological copper-based artifacts. ACS Omega. 2019;4:11103–11.
3. Di Carlo G, Giuliani C, Riccucci C, Pascucci M, Messina E, Fierro G, Lavorgna M, Ingo GM. Artificial patina formation onto copper-based alloys: chloride and sulphate induced corrosion processes. Appl Surf Sci. 2017;421:120–7.
4. Ingo GM, Riccucci C, Giuliani C, Faustoferri A, Pierigè I, Fierro G, Pascucci M, Albini M, Di Carlo G. Surface studies of patinas and metallurgical features of uncommon high-tin bronze artefacts from the Italic necropolises of ancient Abruzzo (Central Italy). Appl Surf Sci. 2019;470:74–83.
5. (5) Moga, T. T. Managing intellectual property in China: a user's guide. Natl Assoc Surf Finish Annu Tech Conf 2006, 910–936.
6. Mezzi A, Angelini E, De Caro T, Grassini S, Faraldi F, Riccucci C, Ingo GM. Investigation of the benzotriazole inhibition mechanism of bronze disease. Surf Interface Anal. 2012;44(8):968–71.
7. Lyon SB, Bingham R, Mills DJ. Advances in corrosion protection by organic coatings: what we know and what we would like to know. Prog Org Coat. 2017;102:2–7.
8. Shchukin DG. Container-based multifunctional self-healing polymer coatings. Polym Chem. 2013;4:4871–7.
9. Zhenhuang T, Shi H, Liu F, Xu S, Han E-H. Inhibiting effect of 8-hydroxyquinoline on the corrosion of silane-based sol-gel coatings on AA 2024-T3. Prog Org Coat. 2015;82:91–100.
10. Kosec T, Škrlep L, Fabjan EŠ, Škapin AS, Masi G, Bernardi E, Chiavari C, Josse C, Esvan J, Robbiola L. Development of multi-component fluoropolymer based coating on simulated outdoor patina on quaternary bronze. Prog Org Coat. 2019;131:27–35.
11. Finšgar M, Milošev I. Inhibition of copper corrosion by 1,2,3-benzotriazole: a review. Corros Sci. 2010;52:2737–49.
12. Giuntoli G, Rosi L, Frediani M, Sacchi B, Salvadori B, Porcinai S, Frediani P. Novel coatings from renewable resources for the protection of bronzes. Prog Org Coat. 2014;77:892–903.
13. Chiavari C, Balbo A, Bernardi E, Martini C, Zanotto F, Vassura I, Bignozzi MC, Monticelli C. Organosilane coatings applied on bronze: influence of UV radiation and thermal cycles on the protectiveness. Prog Org Coat. 2015;82:91–100.
14. Giuliani C, Pascucci M, Riccucci C, Messina E, de Luna MS, Lavorgna M, Ingo GM, Di Carlo G. Chitosan-based coatings for corrosion protection of copper-based alloys: a promising more sustainable approach for cultural heritage applications. Prog Org Coat. 2018;122:138–46.
15. Salzano de Luna M, Buonocore G, Giuliani C, Messina E, Di Carlo G, Lavorgna M, Ambrosio L, Ingo GM. Long-lasting efficacy of coatings for bronze artwork conservation: the key role of layered double hydroxide nanocarriers in protecting corrosion inhibitors from photodegradation. Angew Chem Int Ed. 2018;57:7380–4.
16. Mcnamara CJ, Breuker M, Helms M, Perry TD, Mitchell R. Biodeterioration of incralac used for the pof bronze monuments. J Cult Herit. 2004;5:361–4.
17. Wolfe, J. Deconstructing incralac: a formulation study of acrylic coatings for the protection of outdoor bronze sculpture. *ICOM-CC 18th Triennial Conference* 2017.
18. Wolfe J, Grayburn R. A review of the development and testing of incralac lacquer. J Am Inst Conserv. 2017;56:225–44.
19. Khan PF, Shanthi V, Babu RK, Muralidharan S, Barik RC. Effect of benzotriazole on corrosion inhibition of copper under flow conditions. J Environ Chem Eng. 2015;3:10–9.
20. Carneiro J, Tedim J, Fernandes SCM, Freire CSR, Gandini A, Ferreira MGS, Zheludkevich ML. Chitosan as a smart coating for controller release of corrosion inhibitor 2-mercaptobenzothiazole. ECS Electrochem Lett. 2013;2(6):C19–22.
21. Serdechnova M, Ivanov VL, Domingues MRM, Evtuguin DV, Ferreira MGS, Zheludkevich ML. Photodegradation of 2-mercaptobenzothiazole and 1,2,3-benzotriazole corrosion inhibitors in aqueous solutions and organic solvents. Phys Chem Chem Phys. 2014;16:25152–60.
22. Ma H, Chen S, Yin B, Zhao S, Liu X. Impedance spectroscopic study of corrosion inhibition of copper by surfactants in the acidic solutions. Corros Sci. 2003;45:867–82.

23. Zhang D, Gao L, Zhou G. Inhibition of copper corrosion in aerated hydrochloric acid solution by heterocyclic compounds containing a mercapto group. Corros Sci. 2004;46:3031–40.
24. Voutsa D, Hartmann P, Schaffner C, Giger W. Benzotriazoles, alkylphenols and bisphenol A in municipal wastewaters and in the Glatt River, Switzerland. Environ Sci Pollut Res. 2006;13(5):333–41.
25. Gravgaard M, van Lanschot J. Cysteine as a non-toxic corrosion inhibitor for copper alloys in conservation. J Inst Conserv. 2012;35(1):14–24.
26. Schrekker HS, Silva DO, Gelesky MA, Stracke MP, Schrekker CML, Gonçalves RS, Dupont J. Ether-functionalized imidazolium ionic liquids. J Braz Chem Soc. 2008;19(3):426–33.
27. Li Y, Zhang S, Ding Q, Qin B, Hu L. Versatile 4,6-dimethyl-2-mercaptopyrimidine based ionic liquids as high-performance corrosion inhibitors and lubricants. J Mol Liq. 2019;284:577–85.
28. Dupont J. From molten salts to ionic liquids: a "Nano" journey. Acc Chem Res. 2011;44(11):1223–31.
29. Cai M, Liang Y, Zhou F, Liu W. Tribological properties of novel imidazolium ionic liquids bearing benzotriazole group as the antiwear/anticorrosion additive in poly(ethylene glycol) and polyurea grease for steel/steel contacts. ACS Appl Mater Interfaces. 2011;3:4580–92.
30. Verma C, Ebenso EE, Quraishi MA. Ionic liquids as green and sustainable corrosion inhibitors for metals and alloys: an overview. J Mol Liq. 2017;233:403–14.
31. Harvey TJ, Walsh FC, Nahlé AH. A review of inhibitors for the corrosion of transition metals in aqueous acids. J Mol Liq. 2018;266:160–75.
32. Faraldi F, Cortese B, Caschera D, Di Carlo G, Riccucci C, De Caro T, Ingo GM. Smart conservation methodology for the preservation of copper-based objects against the hazardous corrosion. Thin Solid Films. 2017;622:130–5.
33. Mihelčič M, Perše LS, Šest E, Jerman I, Giuliani C, Di Carlo G, Lavorgna M, Surca AK. Development of solvent- and water-borne fluoropolymer protective coatings for patina-free bronze discs. Prog Org Coat. 2018;125:266–78.
34. Mihelčič M, Gaberšček M, de Luna MS, Lavorgna M, Giuliani C, Di Carlo G, Surca AK. Effect of silsesquioxane addition on the protective performance of fluoropolymer coatings for bronze surfaces. Mater Des. 2019;178:107860–72.
35. Fei Z, Zhao D, Geldbach TJ, Scopelliti R, Dyson PJ. Brønsted acidic ionic liquids and their Zwitterions: synthesis, characterization and PKa determination. Chem Eur J. 2004;10(19):4886–93.
36. Bara EJ, Gabriel JC, Lessmann S, Carlisle KT, Finotello A, Gin LD, Noble DR. Enhanced CO_2 separation selectivity in oligo(ethylene glycol) functionalized room-temperature ionic liquids. Ind Eng Chem Res. 2007;46:5380–6.
37. Shevell SK, editor. The science of color. Amsterdam: Elsevier; 2003.
38. Lavorgna M, Piscitelli F, Mangiacapra P, Buonocore GG. Study of the combined effect of both clay and glycerol plasticizer on the properties of chitosan films. Carbohydr Pol. 2010;82:291–8.
39. La Russa MF, Ruffolo SA, Rovella N, Belfiore CM, Palermo AM, Guzzi MT, Crisci GM. Multifunctional TiO_2 coatings for cultural heritage. Prog Org Coat. 2012;74(1):186–91.
40. La Russa MF, Rovella N, de Buergo MA, Belfiore CM, Pezzino A, Crisci GM, Ruffolo SA. Nano-TiO_2 coatings for cultural heritage protection: the role of the binder on hydrophobic and self-cleaning efficacy. Prog Org Coat. 2016;91:1–8.
41. Giuntoli G, Rosi L, Frediani M, Sacchi B, Salvadori B, Porcinai S, Frediani P. Novel coatings from renewable resources for the protection of bronzes. Prog Org Coat. 2014;77(4):892–903.
42. Zaky MT, Nessim MI, Deyab MA. Synthesis of new ionic liquids based on dicationic imidazolium and their anti-corrosion performances. J Mol Liq. 2019;290:111230.
43. Tomastik J, Ctvrtlik R. Nanoscratch test —a tool for evaluation of cohesive and adhesive properties of thin films and coatings. EPJ Web Conf. 2013;48:00027.
44. Bull SJ. Failure modes in scratch adhesion testing. Surf Coat Techn. 1991;50(1):25–32.
45. Seo TW, Weon JI. Influence of weathering and substrate roughness on the interfacial adhesion of acrylic coating based on an increasing load scratch test. J Mater Sci. 2012;47(5):2234–40.
46. Nessim MI, Zaky MT, Deyab MA. Three new gemini ionic liquids: synthesis, characterizations and anticorrosion applications. J Mol Liq. 2018;266:703–10.
47. Queiroz MF, Teodosio Melo KR, Sabry DA, Sassaki GL, Oliveira Rocha HA. Does the use of chitosan contribute to oxalate kidney stone formation? Mar Drugs. 2015;13(1):141–58.

Publisher's Note